



# Synthesis and distinct urease enzyme inhibitory activities of metal complexes of Schiff-base ligands: Kinetic and thermodynamic parameters evaluation from TG-DTA analysis

Muhammad Ikram<sup>a,b,\*</sup>, Sadia Rehman<sup>a,b</sup>, Faridoon<sup>b</sup>, Robert J. Baker<sup>c</sup>, Hanif Ur Rehman<sup>b</sup>, Ajmal Khan<sup>d</sup>, Muhammad Iqbal Choudhary<sup>d</sup>, Saeed-Ur -Rehman<sup>b</sup>

<sup>a</sup> Department of Chemistry, Sarhad University of Science and Information Technology, Peshawar, Pakistan

<sup>b</sup> Institute of Chemical Sciences, University of Peshawar, Peshawar, Pakistan

<sup>c</sup> School of Chemistry, University of Dublin, Trinity College, Dublin 2, Ireland

<sup>d</sup> H.E.J. Research Institute of Chemistry, International Center for Chemical and Biological Sciences, University of Karachi, Karachi 75270, Pakistan

## ARTICLE INFO

### Article history:

Received 25 October 2012

Received in revised form

14 December 2012

Accepted 30 December 2012

Available online 22 January 2013

### Keywords:

Schiff base coordination compounds

Urease

$\alpha$ -Chymotrypsin

Acetylcholinesterase and

butyrylcholinesterase inhibition

Structure activity relationship (SAR)

Thermal and thermodynamic studies

## ABSTRACT

Transition metal [Co, Ni, Cu and Zn(II) acetates] complexes of salicylaldehyde derived Schiff bases, 2- $\{(E)-[(4\text{-chlorophenyl)imino]methyl}\}$ phenol (**CIMP**) and 2- $\{(E)-[(4\text{-bromophenyl)imino]methyl}\}$ phenol (**BIMP**) were synthesized and characterized by various analytical and spectroscopic studies. The Schiff base ligands and their metal complexes were also screened for their urease,  $\alpha$ -chymotrypsin, acetylcholinesterase and butyrylcholinesterase inhibition activities. The ligands were found active against  $\alpha$ -chymotrypsin with  $IC_{50} \pm S.E.M. = 305.0 \pm 3.2$  and  $330.6 \pm 1.6 \mu M$  respectively. The copper complexes of both the ligands were found active in inhibiting urease enzyme with  $IC_{50} \pm S.E.M. = 10.7 \pm 0.2$  and  $5.0 \pm 0.1 \mu M$  respectively, as compared to standard inhibitor. Structure activity relationship (SAR) was evaluated using autodock programme. It was found that the active complexes block the entrance cavity to the enzyme. All the complexes were evaluated for their thermal degradation studies using TG-DTA analytical methods in static air. Thermodynamic and kinetic parameters were evaluated from the TG/DTA curves using Horowitz–Metzger method.

© 2013 Elsevier B.V. All rights reserved.

## 1. Introduction

The coordination compounds are of considerable interest because metal ions are found in the active sites of a large number of metalloproteins such as hemocyanin, and also in metalloenzymes like in ureases, tyrosinase, laccase and ascorbate oxidase [1–3]. These proteins are involved in various biological processes such as biological electron-transfer reaction, oxygen atom insertion into substrates, dioxygen reduction to hydrogen peroxide or water and hydrolytic reactions. Urease (urea amidohydrolase EC 3.5.15) is a nickel containing metalloenzyme which catalyzes the hydrolysis of urea to ammonia and carbon dioxide. Urease is involved in the function to use urea as nitrogen source [4–6]. Urease is known to be one of the major causes of diseases induced by *Helicobacter pylori*, thus allow them to survive at low pH inside the stomach and thereby, play an important role in the pathogenesis of gastric and peptic ulcer, apart from cancer as well [4]. Urease is directly involved in

the formation of infection stones and contributes to the pathogenesis of urolithiasis, pyelonephritis, and hepatic encephalopathy, hepatic coma and urinary catheter encrustation [7]. In plants urease also act as defense protein in systemic nitrogen transport pathways [3]. Due to the diverse functions of this enzyme, its inhibition by potent and specific compounds could provide an invaluable addition for treatment of infections, and secondary complexes such as pus formation, and ulcer caused by urease-producing bacteria.

$\alpha$ -Chymotrypsin (EC 3.4.21.1), a protease, which is secreted from pancreas, catalyzes the breakdown of polypeptide and proteins. If the precursor of chymotrypsin, the chymotrypsinogens is cleaved to form active enzyme before the target side, then it digest the tissues inside body such as in cases of pancreatitis [8].  $\alpha$ -Chymotrypsin has been found to be involved in clearance of ulcer, digesting damaged tissue and debris in the infected site [9–11]. Selective urease inhibitors which are also not involved in inhibiting  $\alpha$ -chymotrypsin, may enhance the rate of healing of peptic ulcer. Due to this unique feature of action in treating peptic ulcers both urease and  $\alpha$ -chymotrypsin were selected for their inhibitory activities of the synthesized compounds.

Alzheimer's disease (AD) is a degenerative brain disease which destroys the neurons and the connections to the cerebral cortex and

\* Corresponding author at: Department of Chemistry, Sarhad University of Science and Information Technology, Peshawar, Pakistan. Tel.: +92 334 9321879.

E-mail address: [ikram.chemistry@suit.edu.pk](mailto:ikram.chemistry@suit.edu.pk) (M. Ikram).

causes dementia which progresses from short term memory loss to complete immobility [12]. Inhibition of acetylcholinesterase is considered as a promising approach for the treatment of Alzheimer's disease (AD) and for possible therapeutic applications in the treatment of Parkinson's disease, aging, and myasthenia gravis [13–17]. Meanwhile, butyrylcholinesterase (BChE) has been considered to be directly associated with the side effects of the acetylcholinesterase (AChE) inhibitors and the existing drugs for Alzheimer disease (AD). Recent studies have shown that BChE is found in significantly higher quantities in AD plaques than in the plaques of age related non-demented brains. Other relevant studies have also reported that the unfavorable side effect profiles of AChE inhibitors are not associated with their poor selectivity toward AChE [18]. To overcome AD, drugs have been developed which prevent the hydrolysis of the acetylcholine by blocking the acetylcholinesterase (AChE).

Schiff bases play an important role as ligands in metal coordination chemistry even after almost a century since their discovery. Schiff bases and their metal complexes have a variety of biological, clinical, analytical, industrial applications and are playing an important role in catalysis and organic synthesis [19]. Attention is also paid to the design, synthesis, and application of unsymmetrical Schiff base ligands. This interest is developed due to the fact, that in many metalloproteins the metals are in a non-symmetrical environment [20–22]. Schiff bases also offer opportunities for inducing substrate chirality, tuning the metal centered electronic factor, enhancing the solubility and stability of either homogeneous or heterogeneous catalysts [23–28]. The presence of nitrogen and oxygen donor atoms gives special properties to coordination compounds and they can be used effectively and stereospecifically in catalysis for oxidation, reduction and hydrolysis [29]. They are also involved in carcinogenic, antitumour, antiviral and antibacterial activities.

Here we report the coordination complexes of Co(II), Ni(II), Cu(II), and Zn(II) of salicylaldehyde derived Schiff base ligand and their effect on the inhibition of enzymes like urease,  $\alpha$ -chymotrypsin, acetylcholinesterase and butyrylcholinesterase. The activity was studied according to the capability of transition metal complex to inhibit the activities of certain enzymes. Work in this context is of much interest and significance since drugs can be complexed with these metals in order to carry them safely to the receptive site along with decreasing efficacy of certain enzymes.

## 2. Experimental

### 2.1. Materials and methods

All chemicals and solvents used were of Analytical grade. Metal(II) acetates (where metal(II)=Co, Ni, Cu and Zn) obtained from Riedel-de-Haen, and were used without further purification. The partial dehydration of the salts was carried out by drying the hydrated salts in a vacuum oven for several hours at 100–110 °C. Salicylaldehyde was obtained from Acros Organics, other chemicals and enzymes were purchased from Sigma–Aldrich (St. Louis, MO). Unless otherwise stated, all reactions were carried out under dinitrogen atmosphere.

### 2.2. Instrumentation

Elemental analysis was carried out by Varian Elementar II, Germany. Melting points were recorded on electrothermal apparatus. IR spectra were recorded using Shimadzu FTIR Spectrophotometer Prestige-21.  $^1\text{H}$  NMR were taken on Bruker DPX 300 MHz whereas,  $^{13}\text{C}\{^1\text{H}\}$  were recorded on Bruker 75 MHz spectrometer chemical shifts ( $\delta$ ) are given in ppm relative to the residual

solvent protons. UV–vis spectra were recorded on BMS UV-1602. All measurements were carried out at room temperature with freshly prepared solution. Mass spectra were recorded on LCT Orthogonal Acceleration TOF Electrospray mass spectrometer.

### 2.3. Urease inhibition assay

Exact 25  $\mu\text{L}$  of enzyme (jack bean urease) solution and 5  $\mu\text{L}$  of test compounds (0.5 mM concentration) were incubated with 55  $\mu\text{L}$  of buffers containing 100 mM urea for 15 min at 30 °C in each well of 96-well plates. Ammonia production was measured as a urease activity by indophenol method. Final volumes were maintained as 200  $\mu\text{L}$  by adding 45  $\mu\text{L}$  phenol reagent (1%, w/v phenol and 0.005%, w/v sodium nitroprusside), and 70  $\mu\text{L}$  of alkali reagent (0.5%, w/v NaOH and 0.1% active chloride NaOCl) to each well. Using a microplate reader (Molecular Devices, CA, USA), the increase in absorbance was measured at 630 nm after 50 min at pH 6.8 [7].

### 2.4. $\alpha$ -Chymotrypsin inhibition assay

This was performed in 50 mM Tris–HCl buffer pH 7.6 with 10 mM  $\text{CaCl}_2$  according to Cannell et al. [10] with the slight modification.  $\alpha$ -Chymotrypsin (12 units/mL prepared in buffer) with the various concentration of test compound (prepared in DMSO) was incubated at 30 °C for 25 min. The reaction was started by adding *N*-succinyl-L-phenylalanine-*p*-nitroanilide (prepared in buffer) at final concentration of 0.4 mM. The change in absorbance was continuously monitored at 410 nm.

### 2.5. AChE and BChE inhibition assay

AChE Inhibition was determined spectrophotometrically, with acetylthiocholine as substrate, by modifying the method reported by Ellman [30]. The reaction was carried out in 100  $\mu\text{M}$  sodium phosphate buffer (pH 8.0) at 25 °C. In a typical assay, 140  $\mu\text{L}$  of buffer, 20  $\mu\text{L}$  of enzyme preparation, and 20  $\mu\text{L}$  of metal compound solution were mixed and incubated for 30 min. DTNB (10  $\mu\text{L}$ ) was added, and the reaction was initiated by adding 10  $\mu\text{L}$  of acetylthiocholine. Butyrylthiocholine chloride was used as a substrate to assay BChE under similar conditions as above. The rates of hydrolysis of acetylthiocholine and butyrylthiocholine were determined by monitoring the formation of the yellow 2-nitro-5-sulfanybenzoate anion (as a result of the reaction of DTNB with the thiocholine released by the enzymatic hydrolysis) at a wavelength of 412 nm.

### 2.6. Determination of $\text{IC}_{50}$ values

The results (change in absorbance per min) were collected using SoftMax Pro 4.8 software (Molecular Devices, CA, USA). Percentage inhibitions were calculated as follow:  $100 - (\text{OD}_{\text{testwell}}/\text{OD}_{\text{control}}) \times 100$ . The concentrations of test compounds that inhibited the hydrolysis of substrates by 50% ( $\text{IC}_{50}$ ) were determined by monitoring the effect of increasing concentrations of these compounds on the inhibition values. The  $\text{IC}_{50}$  values were then calculated using the EZ-Fit Enzyme Kinetics program (Perrella Scientific Inc., Amherst, USA).

### 2.7. Synthesis of Schiff base ligands

The ligands were prepared according to the reported procedure. 10 mmol of corresponding aniline were taken and reacted at room temperature with 10 mmol salicylaldehyde in 10  $\text{cm}^3$  of ethanol. 2–3 drops of sulfuric acid was added as catalyst. The ligands quickly precipitated out as yellow solid which were filtered and washed

with n-hexane three times. The product was recrystallized from methanol as yellow needles.

### 2.8. 2- $\{(E)-[(4\text{-chlorophenyl)imino]methyl\}$ phenol (**CIMP**)

Yield; 75%, m.p. 93–95 °C elemental analysis,  $C_{13}H_{10}ClNO$ . Calc. C: 67.39%, H: 4.35%, N: 6.05%, Exp. C: 67.90%, H: 4.30%, N: 6.57%, IR analysis: 3400(bd), 1683(s), 1608(s), 1485(s), 1456(s), 1394(w), 1271(s), 1149(s), 1010(s), 908(w), 835(s), 813(s), 754(s), 698(s), 630(w)  $cm^{-1}$ ,  $^1H$  NMR (300.13 MHz,  $CDCl_3$ , 303k)  $\delta$  = 6.9 (d,  $^3J_{HH}$  = 7.2 Hz, 1H, H12), 7.04 (d,  $^3J_{HH}$  = 7.23 Hz, 1H, H15), 7.1 (d,  $^3J_{HH}$  = 7.56 Hz, 1H, H14 and H13), 7.4 (d,  $^3J_{HH}$  = 7.01 Hz, 1H, H3 and H5), 7.5 (d,  $^3J_{HH}$  = 7.25 Hz, 1H, H2 and H6), 8.6 (s, Ar– $\underline{HC=N}$ ), 13.0 (s, OH),  $^{13}C\{^1H\}$  NMR (75.47 MHz,  $CDCl_3$ , 303k), 117.3 (CH, C15), 119.0 (CH, C13), 119.2 (CH, C14), 122.4 (CH, C2 and C6), 129.5 (CH, C3 and C5), 132.4 (CH, C12), 133.48 (C, C4), 147.0 (C, C1), 161.1 (C, C11), 162.9 (CH, Ar– $\underline{HC=N}$ ).

### 2.9. 2- $\{(E)-[(4\text{-bromophenyl)imino]methyl\}$ phenol (**BIMP**)

Yield; 80%, m.p. 90–92 °C elemental analysis,  $C_{13}H_{10}BrNO$ . Calc. C: 56.55%, H: 3.65%, N: 5.07%, IR analysis: 3400(bd), 1606(s), 1568(s), 1481(s), 1409(s), 1359(s), 1280(s), 1184(s), 1151(s), 1107(s), 1006(s), 983(s), 910(s), 852(s), 752(s), 678(s)  $cm^{-1}$ .  $^1H$  NMR (300.13 MHz,  $CDCl_3$ , 303k)  $\delta$  = 6.9 (d,  $^3J_{HH}$  = 7.01 Hz, 1H, H12), 7.03 (d,  $^3J_{HH}$  = 7.2 Hz, 1H, H15), 7.1 (d,  $^3J_{HH}$  = 7.34 Hz, 1H, H14 and H13), 7.4 (d,  $^3J_{HH}$  = 6.8 Hz, 1H, H3 and H5), 7.5 (d,  $^3J_{HH}$  = 7.9 Hz, 1H, H2 and H6), 8.6 (s, Ar– $\underline{HC=N}$ ), 13.0 (s, OH),  $^{13}C\{^1H\}$  NMR (75.47 MHz,  $CDCl_3$ , 303k), 117.3 (CH, C3 and C5), (CH, C15), 119.0 (CH, C13), 119.2 (CH, C14), 122.8 (CH, C2 and C6), 132.4 (CH, C12), 133.5 (C, C4), 147.4 (C, C1), 161.1 (C, C11), 162.9 (CH, Ar– $\underline{HC=N}$ ).

### 2.10. Synthesis of complexes

10 mmol of the Schiff base ligand in 10  $cm^3$  of dried methanolic solution was added to the dehydrated methanolic solution of 0.4 mmol metal salts and stirred the mixture for 3–6 h. Partial dehydration of the metal salts was achieved by keeping the metal salts in oven at 105 °C for 3 h. These metal salts were dissolved in 10  $cm^3$  dried methanol and excess dimethoxy propane was added to it to achieve the complete dehydration. On mixing the metal salt solution with ligand solutions, the complexes either precipitated instantaneously otherwise obtained by concentrating the solutions using rotary evaporator. The product was washed with 10% copious methanol containing n-hexane solution.

### 2.11. Bis(2- $\{(E)-[(4\text{-chlorophenyl)imino]methyl\}$ phenolate)nickel(II) (**1**)

Yield; 55%, m.p. 248–250 °C elemental analysis,  $C_{26}H_{18}Cl_2N_2NiO_2$ . Calc. C: 60.05%, H: 3.49%, N: 5.39% Ni: 11.29%, MS-ES<sup>+</sup>:  $m/z$  (%) = 540.9997 (100%) [ $C_{26}H_{18}Cl_2N_2NiO_2+Na$ ], IR analysis: 3303(bd), 1611(s), 1531(s), 1466(s), 1444(s), 1418(s), 1349(s), 1330(s), 1258(s), 1220(s), 1188(s), 1142(s), 1142(s), 1116(s), 1023(w), 976(s), 938(s), 901(s), 862(w), 812(s), 806(s), 759(s), 748(s), 721(s), 698(s), 667(s)  $cm^{-1}$ ,  $\lambda_{max}$  = 710 nm ( $\epsilon$  = 27.7  $M^{-1} cm^{-1}$ ,  $^1A_{1g} \rightarrow ^1A_{2g}$ ).

### 2.12. Bis(2- $\{(E)-[(4\text{-chlorophenyl)imino]methyl\}$ phenolate)cobalt(II) (**2**)

Yield; 75%, m.p. 270–272 °C elemental analysis,  $C_{26}H_{18}Cl_2CoN_2O_2$ . Calc. C: 60.02%, H: 3.49%, Co: 11.33% N: 5.38%, MS-ES<sup>+</sup>:  $m/z$  (%) = 519.0075 (100%) [ $C_{26}H_{18}Cl_2CoN_2O_2^+$ ], IR analysis: 1606(s), 1537(s), 1485(s), 1463(s), 1440(s), 1379(s), 1325(s), 1178(s), 1149(s), 1126(s), 1089(s), 1012(s), 979(s), 925(s), 856(s),

831(s), 759(s), 696(s)  $cm^{-1}$ ,  $\lambda_{max}$  = 890 nm ( $\epsilon$  = 16.6  $M^{-1} cm^{-1}$ ,  $^2A_{2g} \rightarrow ^2B_{1g}$ ).

### 2.13. Bis(2- $\{(E)-[(4\text{-chlorophenyl)imino]methyl\}$ phenolate)copper(II) (**3**)

Yield; 68%, m.p. 219–220 °C elemental analysis,  $C_{26}H_{18}Cl_2CuN_2O_2$ . Calc. C: 59.49%, H: 3.46%, Cu: 12.11%, N: 5.34%, MS-ES<sup>+</sup>:  $m/z$  (%) = 545.9939 (100%) [ $C_{26}H_{18}Cl_2CuN_2O_2+Na$ ], IR analysis: 1598(s), 1573(s), 1519(s), 1489(s), 1431(s), 1390(s), 1348(s), 1321(s), 1300(s), 1249(s), 1211(w), 1170(s), 1147(s), 1126(s), 1093(s), 1029(s), 1006(s), 975(s), 923(s), 852(s), 827(s), 756(s), 696(s), 610(s)  $cm^{-1}$ ,  $\lambda_{max}$  = 690 nm ( $\epsilon$  = 220.6  $M^{-1} cm^{-1}$ ,  $d_{z^2} \rightarrow d_{x^2-y^2}$ ).

### 2.14. Bis(2- $\{(E)-[(4\text{-chlorophenyl)imino]methyl\}$ phenolate)zinc(II) (**4**)

Yield; 55%, m.p. 278–280 °C elemental analysis,  $C_{26}H_{18}Cl_2ZnN_2O_2$ . Calc. C: 59.28%, H: 3.44%, N: 5.32%, Zn: 12.42%, MS-ES<sup>+</sup>:  $m/z$  (%) = 524.0063 (80%) [ $C_{26}H_{18}Cl_2ZnN_2O_2^+$ ], IR analysis: 1598(s), 1581(s), 1521(s), 1460(s), 1435(s), 1394(s), 1348(s), 1325(s), 1249(s), 1170(s), 1147(s), 1093(s), 1029(s), 1006(s), 923(s), 827(s), 786(s), 756(s), 698(s), 590(s)  $cm^{-1}$ .

### 2.15. Bis(2- $\{(E)-[(4\text{-bromophenyl)imino]methyl\}$ phenolate)nickel(II) (**5**)

Yield; 83%, m.p. 100–102 °C elemental analysis,  $C_{26}H_{18}Br_2N_2NiO_2$ . Calc. C: 51.28%, H: 2.98%, N: 4.60%, Ni: 9.64%,  $m/z$  (%) = 605.5830 (100%) [ $C_{26}H_{18}Br_2NiO_2^+$ ], IR analysis: 1611(s), 1531(s), 1466(s), 1444(s), 1418(s), 1349(s), 1330(s), 1258(s), 1220(s), 1188(s), 1142(s), 1142(s), 1116(s), 1023(w), 976(s), 938(s), 901(s), 862(w), 812(s), 806(s), 759(s), 748(s), 721(s), 698(s), 667(s)  $cm^{-1}$ ,  $\lambda_{max}$  = 890 nm ( $\epsilon$  = 16.6  $M^{-1} cm^{-1}$ ,  $^1A_{1g} \rightarrow ^1A_{2g}$ ).

### 2.16. Bis(2- $\{(E)-[(4\text{-bromophenyl)imino]methyl\}$ phenolate)cobalt(II) (**6**)

Yield; 75%, m.p. 230–232 °C elemental analysis,  $C_{26}H_{18}Br_2CoN_2O_2$ . Calc. C: 51.26%, H: 2.98%, Co: 9.67%, N: 4.60%,  $m/z$  (%) = 606.7541 (100%) [ $C_{26}H_{18}Br_2CoN_2O_2^+$ ], IR analysis: 1683(w), 1653(s), 1604(s), 1533(s), 1483(w), 1463(s), 1446(s), 1379(s), 1348(s), 1327(s), 1253, 1180(s), 1149(s), 1072(s), 1010(s), 925(s), 856(s), 831(s), 761(s), 711(s), 678(s)  $cm^{-1}$ ,  $\lambda_{max}$  = 790 nm ( $\epsilon$  = 16.6  $M^{-1} cm^{-1}$ ,  $^2A_{2g} \rightarrow ^2B_{1g}$ ).

### 2.17. Bis(2- $\{(E)-[(4\text{-bromophenyl)imino]methyl\}$ phenolate)copper(II) (**7**)

Yield; 71%, m.p. 276–278 °C elemental analysis,  $C_{26}H_{18}Br_2CuN_2O_2$ . Calc. C: 50.88%, H: 2.96%, Cu: 10.35%, N: 4.56%,  $m/z$  (%) = 611.1259 (90%) [ $C_{26}H_{18}Br_2CuN_2O_2+H^+$ ], IR analysis: 1597(s), 1570(s), 1521(s), 1490(s), 1460(s), 1429(s), 1388(s), 1348(s), 1321(s), 1249(s), 1209(s), 1170(s), 1147(s), 1126(s), 1078(s), 1029(s), 1002(s), 975(s), 925(s), 852(s), 823(s), 786(s), 756(s), 677(s)  $cm^{-1}$ .  $\lambda_{max}$  = 690 nm ( $\epsilon$  = 220.6  $M^{-1} cm^{-1}$ ,  $d_{z^2} \rightarrow d_{x^2-y^2}$ ).

### 2.18. Bis(2- $\{(E)-[(4\text{-bromophenyl)imino]methyl\}$ phenolate)zinc(II) (**8**)

Yield; 45%, m.p. 278–280 °C elemental analysis,  $C_{26}H_{18}Br_2ZnN_2O_2$ . Calc. C: 50.72%, H: 2.95%, N: 4.55%, Zn: 10.62%,  $m/z$  (%) = 611.3404 (100%) [ $C_{26}H_{18}Br_2ZnN_2O_2^+$ ], IR analysis:

1595(w), 1523(w), 1460(s), 1436(s), 1394(s), 1325(w), 1301(w), 1170(w), 1147(s), 1078(w), 983(w), 923(w), 825(w), 758(s), 667(s), 634(s)  $\text{cm}^{-1}$ .

### 2.19. Docking

The crystal structure of urease from *Bacillus pasteurii* was downloaded from protein data bank (PDB code: 4UBP). Pymol was used to remove water molecules and non-standard protein residues from the urease enzyme. Then Autodock Tools was used to add polar hydrogen atoms, and assign charges with the Gasteiger method, define the active sites and to save the structure of the enzyme as receptor into the required pdbqt format. The docking site on the receptor macromolecule was defined by fixing the grid box with the dimensions  $40 \text{ \AA} \times 40 \text{ \AA} \times 40 \text{ \AA}$  with grid spacing of  $0.375 \text{ \AA}$  centered on Ni841 in the active site of the protein. Then ten runs with AutoDock Vina [33] were performed and the best pose was saved.

### 2.20. TG-DTA analysis

The TG-DTA analyses were carried out using TG/DTA Diamond model by Perkin Elmer at heating rate  $10^\circ\text{C min}^{-1}$  in temperature range  $30\text{--}1000^\circ\text{C}$  under static air. Specific mass of samples were contained in ceramic pans crucibles adjusted on platform support giving a proportional signal to recorder, observed by computer interface and the results were plotted in the form of mass loss of sample vs. temperature for TG and microvolts vs. temperature for DTA. All the results were referenced to thermal decomposition of alumina. The activation energies of all the samples were calculated using Horowitz–Metzger method [34]. It was found that linear plots can be obtained while  $\ln \ln(W_0 - W_t^f / (W - W_t^f))$  {where  $W_0$  = initial mass taken,  $W$  = weight remaining at a given temperature,  $W_t^f$  = final weight} were plotted against  $\theta$  {where  $\theta = T_c - T_s$ }. The slope of the straight line was used to calculate the activation energy through the expression (1):

$$\text{Slope} = \frac{Ea}{RT_s^2} \quad (1)$$

Order of decomposition was calculated from the relationship between reaction order and concentration at maximum slope [34]. Thermodynamic parameters of activation were evaluated by using the following expressions (2)–(4), respectively [35]:

$$\Delta S^* = 2.303 \log \left[ \frac{Ah}{k_B T_s} \right] R \quad (2)$$

$$\Delta H^* = \Delta Ea - RT \quad (3)$$

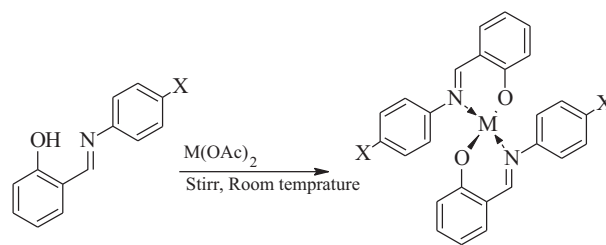
$$\Delta G^* = \Delta H^* - T\Delta S^* \quad (4)$$

## 3. Result and discussion

### 3.1. Chemistry

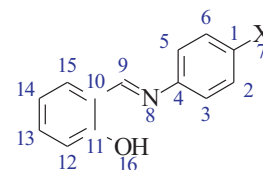
Schiff base of the pharmacologically important salicylaldehyde was prepared by condensing one equivalent of 4-chloro or bromo substituted anilines with one equivalent of the aldehyde. The two ligands were isolated in 75–80% yields. The uncorrected melting points for both the ligands were found to be in the range of  $90\text{--}95^\circ\text{C}$ . Both these Schiff base ligands were reacted with transition metal ions like Co(II), Ni(II), Cu(II) and Zn(II) in 2:1 equivalent ratios and obtained their corresponding metal complexes with composition  $[M(\text{CIMP or BIMP})_2]$  as shown in Scheme 1.

The two Schiff base ligands and their metal complexes were completely characterized by various characterization techniques. Elemental analysis and ES(+) mass spectral data suggest the characteristic compositions in which the metal center is surrounded by



Where X = Cl, Br and M = Co, Ni, Cu and Zn

**Scheme 1.** Metal complexes of the Schiff bases **CIMP** and **BIMP**.



Where X = Br, Cl

**Fig. 1.** Scheme for NMR signal assignment.

two anionic ligands.  $^1\text{H}$  and  $^{13}\text{C}\{^1\text{H}\}$  NMR for both the Schiff base ligands were measured and all the peaks assigned unambiguously. The representative imine linkage peak was observed at 8.6 ppm in  $^1\text{H}$  NMR of both the ligands. The peak for the imine carbon is observed at 162.9 ppm in  $^{13}\text{C}\{^1\text{H}\}$  NMR. Rest of the splitting pattern peak values for all the protons and carbons are assigned and given. Fig. 1 represents the atomic numbering scheme for the ligands. Infrared spectra for the ligands and metal complexes were measured in the region of  $4000\text{--}600 \text{ cm}^{-1}$  in relation to the structure. The infrared spectral data show the disappearance of broad hydroxyl peak in the free ligands and also a change in the  $\text{C}=\text{N}$  absorption frequency. Therefore it is unambiguously assigned that the skeleton of the complexes is produced by these two coordinating sites. All the complexes were found to be non-electrolyte as the values suggest which is attributed to the absence of free acetate ions.

The UV–vis spectra of compounds **1**, **3**, **5**, and **7** were measured in spectrophotometric grade ethanol within the region of  $400\text{--}800 \text{ nm}$  whereas these were measured in spectrophotometric grade within the range of  $400\text{--}1000 \text{ nm}$  for **2** and **6** respectively. **1** and **5** compounds show the same trend of absorption which was assigned to  $^1\text{A}_{1g} \rightarrow ^1\text{A}_{2g}$  square planar transition, whereas the other absorption transitions  $^1\text{A}_{1g} \rightarrow ^1\text{B}_{1g}$  and  $^1\text{A}_{1g} \rightarrow \text{E}_g$  were considered to be buried in the same  $^1\text{A}_{1g} \rightarrow ^1\text{A}_{2g}$  transition. Similarly for **2** and **6** the absorption was assigned to the transition  $^2\text{A}_{2g} \rightarrow ^2\text{B}_{1g}$  for  $\text{C}_{2v}$  symmetry. In case of copper as may be seen by looking into the absorption band in **3** and **7**, the transition band is assigned to  $d_{z^2} \rightarrow d_{x^2-y^2}$ . In all of the compounds the transitions were assigned as ligand to metal charge transfer (LMCT) transitions.

### 3.2. Enzyme inhibitory studies

The metal complexes have been extensively used as therapeutics in many physiological disorders. Bismuth complexes are one of them widely used for the treatment of peptic ulcers and *H. pylori* infections as urease inhibitors [31]. Bismuth has exhibited many side effects such as darkening of tongue, vomiting, diarrhea, and dizziness. To overcome these side effects we have synthesized various metal complexes of Schiff-base and they were checked for their potential inhibition against urease enzyme. The most interesting and excellent activity were shown by Cu-complexes with

**Table 1**  
Enzyme inhibitory efficacy of the Schiff base and their metal complexes.

Compound	Urease (IC <sub>50</sub> ± S.E.M. <sup>b</sup> ) (μM)	α-Chymotrypsin (IC <sub>50</sub> ± S.E.M.) (μM)	Acetylcholinesterase (IC <sub>50</sub> ± S.E.M.) (μM)	Butyrylcholinesterase (IC <sub>50</sub> ± S.E.M.) (μM)
<b>CIMP</b>	NA <sup>a</sup>	305.04 ± 3.24	NA	NA
<b>1</b>	NA	NA	NA	NA
<b>2</b>	NA	NA	NA	NA
<b>3</b>	10.66 ± 0.19	NA	NA	NA
<b>4</b>	NA	NA	NA	NA
<b>BIMP</b>	NA	330.55 ± 1.60	NA	NA
<b>5</b>	NA	NA	NA	NA
<b>6</b>	NA	NA	NA	NA
<b>7</b>	5.0 ± 0.05	NA	NA	NA
<b>8</b>	NA	NA	NA	NA
Thiourea <sup>c</sup>	21 ± 0.011	–	–	–
Chymostatin <sup>d</sup>	–	5.71 ± 0.13	–	–

<sup>a</sup> NA = not active, i.e., % of inhibition is less than 50% at 500 μM.

<sup>b</sup> S.E.M. = standard error of mean.

<sup>c</sup> Standard inhibitor of urease.

<sup>d</sup> Standard inhibitor of α-chymotrypsin.

both ligands HL<sub>1</sub> and HL<sub>2</sub> which reveal that Cu based complexes of both series will be excellent in this therapy. The Cu-complex of first series ([Cu(**CIMP**)<sub>2</sub>]) have IC<sub>50</sub> 10.66 ± 0.19 μM while the Cu-complex of second series ([Cu(**BIMP**)<sub>2</sub>]) have IC<sub>50</sub> 5 ± 0.047 μM which are two and four time more better than our standard thiourea (IC<sub>50</sub> 21 ± 0.011 μM) the results are in Table 1. As we know that α-chymotrypsin is also involved in ulcer healing [7] so, we subjected the same complexes to the α-chymotrypsin inhibitory activity. Bare Schiff-base ligands were found to be inactive to moderately active in urease and α-chymotrypsin, respectively. Only copper complexes of both the ligands showed inhibition toward urease enzyme. Neither ligand nor their complexes found to be inhibiting acetylcholinesterase (AChE) and butyrylcholinesterase (BChE) enzymes. The results are shown in Table 1.

### 3.3. Molecular docking study

The 3D structure of urease from *B. pasteurii* (entry 4UBP in the Protein Data Bank) contains two Ni ions in the active sites. Ni(1) is coordinated by His249 (2.0 Å) and His275 (2.0 Å), while Ni(2) is coordinated by His137 (2.0 Å), His139 (2.0 Å), and Asp363 (2.1 Å). The 3D structure, and the binding distances between Ni ions and their coordinated residues are shown (see Supplementary materials).

The enzyme surface model for the complexes **3** and **7** revealed that these complexes **3** and **7** are well filled in the active pocket of the urease. The complexes formed hydrophobic interactions with Ala170, Cys322 and His323 of the urease resulting in the blockage of the active pocket of the enzyme. Entrance of the other species is hence effected that is possibly giving rise to the activities of the complexes **3** and **7** respectively. These results also that the chloro and bromo substitution on the Schiff base ligands are not so much effective that can dictate the enzyme inhibition.

**Table 2**  
Thermodynamic parameters of metal complexes.

Compound	T <sub>s</sub> (K)	E <sub>a</sub> (kJ/mol)	ΔH <sup>‡</sup> (kJ/mol)	ΔG <sup>‡</sup> (kJ/mol)	ΔS <sup>‡</sup> (J mol <sup>-1</sup> K <sup>-1</sup> )	Order of reaction (n)
<b>CIMP</b>	524.9	89.09	84.72	209.71	–238.13	1
<b>1</b>	603	9.06	4.04	167.31	–254.19	5
<b>2</b>	517.6	26.95	22.64	164.89	–258.19	4
<b>3</b>	636.7	11.80	6.50	170.73	–257.94	∞
<b>4</b>	649	8.75	3.35	168.39	–254.30	∞
<b>BIMP</b>	543	13.00	8.48	124.73	–214.10	∞
<b>5</b>	837	16.89	9.93	220.19	–251.18	½
<b>6</b>	617	12.97	7.84	167.04	–258.03	∞
<b>7</b>	678	8.79	3.15	173.05	–250.59	5
<b>8</b>	821.8	25.26	18.42	222.04	–247.78	3

Earlier study in this field represent that copper complexes of the Schiff base ligands derived from naphthaldehyde and various amines are also active against urease. It was found that copper complexes of the Schiff base ligands were much more effective in inhibiting the urease activity as compared to the standard drug [32]. Exceptional activities were observed when there is no halogen substitution on the ligand which lowers the binding energy appreciably lower than the expected [32].

### 3.4. Thermodynamics and thermal studies

Thermal degradation of Schiff base ligands **CIMP** and **BIMP** and their corresponding metal complexes were studied in the range of 30–1000 °C except **1** and **2** metal complexes, studied up to 1200 °C. Table 2 show the temperature at which maximum loss of the species under study occurred, this temperature is called temperature at maximum slope and represented by T<sub>s</sub>. Activation energies of all the compounds were calculated using Horowitz and Metzger method of calculations. From this data order of degradation was calculated using the relationship between reaction order and concentration at maximum slope [11]. Thermodynamic parameters were calculated using the relationships given in Section 2.20.

TG and DTA curves for metal complexes of both **BIMP** and **CIMP** are shown in Figs. 2–5 respectively. Table 3 depicts the species which are evolved during each thermo gravimetric step. Differential thermo gravimetric values for each thermo gravimetric step are given. By looking into Table 3 it is apparent that both the Schiff base ligands are pyrolyzed in a single step producing 4-halo substituted biphenol and hydrogen cyanide. Degradation starts at 190 °C in **CIMP**, whereas in **BIMP** it starts at 210 °C. The theoretical and experimental calculated weights of the moieties are similar with three DTA peaks. **CIMP** follow 1st order degradation kinetics whereas **BIMP** infinite order, clearly points to the electronic effects

**Table 3**  
Thermo analytical results of H-QMP and its complexes.

Compound	TG temp. range (°C)	Stage	Mass loss		DTA	Moieties evolved
			% Calc.	% Found		
<b>CIMP</b>	30–280	I	100	100	(-)12.3, (-)15.14, (-)13.5	HCN, C <sub>12</sub> H <sub>9</sub> ClO
	30–390	I	55.8	55.6	(-)36, (+)2	C <sub>12</sub> H <sub>9</sub> ClO, 2CO, H <sub>2</sub> , N <sub>2</sub>
	390–1000	II	39.1	38.21	(-)26	C <sub>12</sub> H <sub>9</sub> ClO
	>1000	Res	11.1	10.72	-	NiO
<b>1</b>	30–410	I	22.9	22.5	(-)40, (-)23, (-)20	2CO, 2H <sub>2</sub> O, N <sub>2</sub>
	410–670	II	78.6	70.4	(-)19.0, (+)18, (+)20, (+)23	2C <sub>12</sub> H <sub>9</sub> ClO
	670–980	III	5.8	6.1	(-)58	O <sub>2</sub>
	>980	Res	11.2	11.0	-	Co
<b>2</b>	30–360	I	16.7	17.8	(-)2, (-)34, (-)18	2CO, H <sub>2</sub> , N <sub>2</sub>
	360–660	II	77.8	73.8	(+)20	2C <sub>12</sub> H <sub>9</sub> ClO
	660–910	III	6.0	6.5	(-)59	O <sub>2</sub>
	>910	Res	11.9	11.5	-	Cu
<b>3</b>	30–430	I	34.1	34.2	(-)8, (-)28	2CO, H <sub>2</sub> , N <sub>2</sub> , C <sub>6</sub> H <sub>6</sub> O
	430–970	II	61.9	59.6	(-)18, (-)29	C <sub>17</sub> H <sub>12</sub> Cl <sub>2</sub> O
	>970	Res	12.2	9.0	-	Zn
<b>BIMP</b>	30–880				(-)5.4, (-)4.5, (-)8.5, (-)7.4, (-)6, (-)9.8	HCN, C <sub>12</sub> H <sub>9</sub> BrO
	30–220	I	15.4	16.0	(-)8	2H <sub>2</sub> O, 2HCN
	220–480	II	80.2	79.8	(-)23, (-)21, (-)26	2C <sub>12</sub> H <sub>9</sub> BrO
	>480	Res	9.5	9.1	(+)12	Ni
<b>4</b>	30–380	I	14.2	15.0	(-)28	2CO, N <sub>2</sub> , H <sub>2</sub>
	380–960	II	82.1	80.3	(+)43	2C <sub>12</sub> H <sub>9</sub> BrO
	>960	Res	28.9	27.5	-	Co <sub>2</sub> O <sub>3</sub>
<b>5</b>	30–380	I	15.0	17.1	(-)2, (-)20, (-)18	2CO, N <sub>2</sub> , H <sub>2</sub>
	380–700	II	80.7	76.8	(-)36, (+)24	2C <sub>12</sub> H <sub>9</sub> BrO
	>700	Res	13.4	14.9	-	CuO
<b>6</b>	30–380	I	24.1	23.1	(-)2, (-)24	CH <sub>3</sub> Cl, 2HCN
	380–800	II	78.4	75.3	(-)18, (-)17, (+)14, (-)14	2C <sub>6</sub> H <sub>5</sub> Br, 2C <sub>6</sub> H <sub>6</sub> O
	>800	Res	10.5	9.8	-	Zn

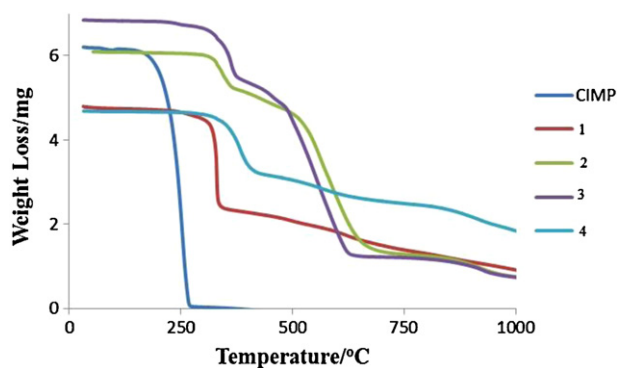


Fig. 2. Thermogravimetric plots of **CIMP** and its metal complexes.

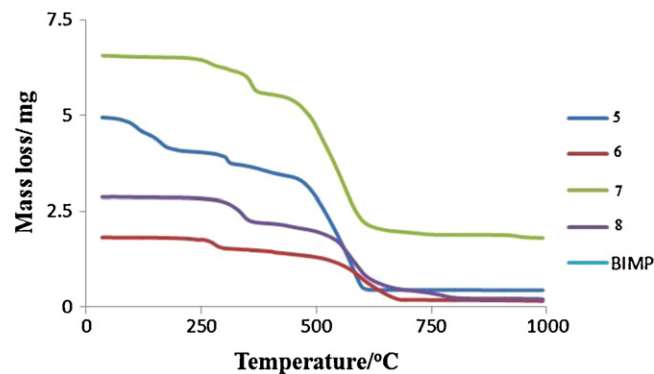


Fig. 4. Thermogravimetric plots of **BIMP** and its metal complexes.

of the halogen groups. **CIMP** has 89.09 kJ/mol activation energy values, whereas the activation energy for **BIMP** is 13.0 kJ/mol. This type of difference can also be seen in the values of enthalpy change and Gibb's free energy change. Both the ligands have negative entropies

depicting that the degradation is less favorable of the parent compounds. By observing the clear demarcated change in the values of entropy change, enthalpy change, Gibb's free energy change, activation energy and most importantly the order of the degradation it becomes apparent that chloro substituted Schiff base ligand is more

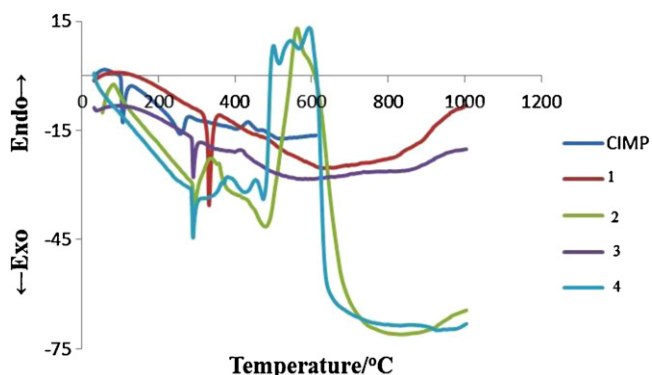


Fig. 3. Differential thermogravimetric curves for **CIMP** and its metal complexes.

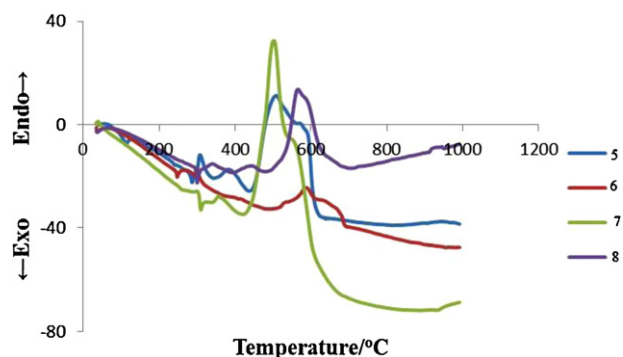


Fig. 5. Differential thermogravimetric curves for **BIMP** and its metal complexes.



**Scheme 2.** Thermal degradation of **CIMP**.



**Scheme 3.** Thermal degradation of **BIMP**.

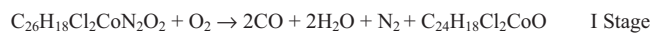
stable than the bromo analog. This type of change in behavior can be observed in other properties as well. The degradation of **CIMP** and **BIMP** follows the following Schemes 2 and 3 respectively:

In **1**,  $T_s$  is around 603 °C which depicts the loss of 4-chlorobiphenol, produced by the fusion of two free radicals, i.e., chlorobenzene free radical and hydroxybenzene free radical. This fusion is shown by –26 DTA peak. The activation energy for **1** is 9.06 kJ/mol and follow 5th order kinetics of degradation. In the first step two moles of carbon monoxide, one mole of nitrogen and hydrogen molecules along with one mole of 4-chlorobiphenol are released. The second stage starts around 400 °C and completes at 1000 °C. This stage is associated with the release of one mole of 4-chlorobiphenol moiety. Nickel oxide remains as residue which was confirmed by taking the IR study. A sharp band was observed around 405  $\text{cm}^{-1}$ . Collectively there are three DTA peaks which support the formation of three intermediate products, i.e., chlorobenzene free radical, hydroxybenzene free radical and hydrogen cyanide molecule. Chlorobenzene free radical and hydroxybenzene free radical bonds together and produce 4-chlorobiphenol, whereas hydrogen cyanide is converted to carbon monoxide, hydrogen gas and nitrogen gas. The low enthalpy change, large Gibb's free energy and negative entropy depict the stable nature of parent compounds rather the degradation products. The degradation is shown in Scheme 4.

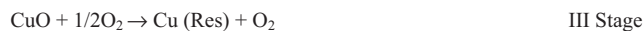
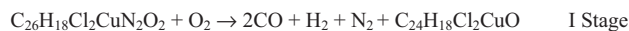
Compound **2** degrades in three steps unlike **1**. The degradation starts around 360 °C and completes at 1000 °C. The decomposition of **2** occurs around 370 °C along with the release of two moles of carbon monoxide, two moles of water and one mole of dinitrogen gas. Second stage of decomposition is associated with the release of two moles of 4-chlorobiphenol. In the third stage the decomposition of the cobalt oxide produced the residual cobalt metal by the release of oxygen molecule. First stage is associated with exothermic DTA peak at –40 and two endothermic peaks at –20 and –23. The exothermic peak represents the initiation of decomposition whereas the two shoulder peaks represent the intermediate hydrogen cyanide which reacts with air to produce one mole each of diatomic gases of nitrogen and hydrogen and two moles of carbon monoxide. The third stage is associated with the weak exothermic peak at –58. The degradation follows the 4th order kinetics.

The activation energy for the thermal degradation is also higher than **1**, i.e., 26.96 kJ/mol. Gibb's free energy change is high, entropy is negative and almost equal to **5** but enthalpy is higher than **1** representing the stable nature of the parent compound. Thermal degradation of **2** is shown in Scheme 5.

In **3**, the thermal degradation starts around 280 °C and completes at 1000 °C leaving copper as residue. Thermal degradation of the compound is comprised three stages. First stage is represented by the formation of two moles of carbon monoxide, one mole each of dihydrogen and dinitrogen. This stage shows three DTA peaks, one exothermic around –38 and two shoulder endothermic peaks around –19. Second stage starts at 410 °C and completes



**Scheme 5.** Thermal degradation of **2**.



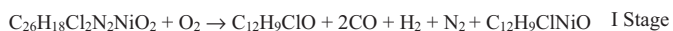
**Scheme 6.** Thermal degradation of **3**.

around 670 °C with three DTA peaks. This stage is represented by the release of two moles of 4-chlorobiphenol. There is one large endothermic peak for this stage. The third stage like **2**, is comprised the CuO degradation releasing dioxygen. There is no DTA peak for this stage. In Table 3, 11.80 kJ/mol is the activation energy for **3**, and follow infinite order of degradation. The entropy is negative than **1** and almost equal to **2**. Similar behavior is followed in Gibb's free energy, but enthalpy change is contrasting in nature. These thermodynamic parameters reveal that copper complex of **CIMP** ligand is stable than its nickel and cobalt analogs. Thermal degradation of **3** is shown in the form of Scheme 6.

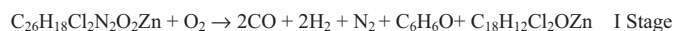
Compound **4** of the **CIMP** series is behaving differently than other compounds with different metal centers. Thermal degradation is completed in two steps with zinc as residue. The first stage is marked and clear, starts at almost 400 °C and completes 440 °C. In this stage, two moles of carbon monoxide, two moles of dihydrogen, one mole of dinitrogen and one mole of phenol ion are produced. The second stage of thermal degradation is comprised many encompassing steps which may be partly due to the formation of free radicals and partly because of fusion of these free radicals with each other. This stage show two DTA peaks both of them are endothermic, clearly reveal the presence of two major intermediate products. These two products are two 4-chlorobenzene free radicals and one phenolic free radical. All these may combine and rearrange to produce 4,4'-dichloro-1,1':3',1''-terphenyl-2'-ol, a stable product produced by the ortho substituting effect of phenolate ion. Compound **4** has negative entropy which is almost equal to **1**. This change in entropy value suggests that parent compound is much more favorable than the degradation. Subsequent trend in Gibb's free energy change and enthalpy change were observed. The thermal degradation of **4** follows the following in Scheme 7.

Overall based upon the  $T_d$  values it become clear that  $\text{Zn(II)} > \text{Ni(II)} > \text{Co(II)} > \text{Cu(II)}$  whereas based on the activation energies it is clear that  $E_{a2} > E_{a3} > E_{a1} > E_{a4}$ .

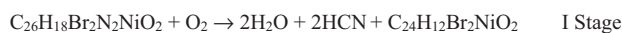
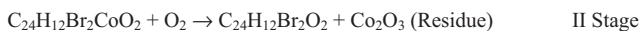
Compound **5** starts decomposition at around 220 °C which subsequently completes at 610 °C. The overall decomposition takes two steps to complete. In the first step two moles of water molecules and two moles of hydrogen cyanide molecules from the Schiff base linkage are produced. Only one endothermic peak is observed in this stage due to the melting of the parent compound. The second and final stage of pyrolysis is comprised production of two moles of 4-bromobiphenolate ion. This stage of decomposition



**Scheme 4.** Thermal degradation of **1**.



**Scheme 7.** Thermal degradation of **4**.

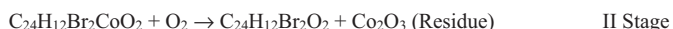
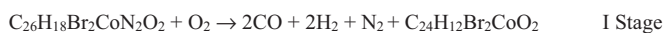
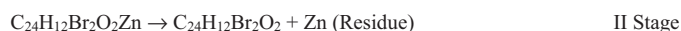
**Scheme 8.** Thermal degradation of **5**.**Scheme 9.** Thermal degradation of **6**.

starts after the end of the first stage and completes at 610 °C. This stage of decomposition is comprised small encompassing steps due to the intermediate free radicals formation. These free radicals are 4-bromobenzene and 2-hydroxybenzene. They bond together to produce the 4-bromobiphenolate ion and evaporates without further decomposition leaving behind residue in the form of nickel. This free radical reaction is represented by the appearance of a huge endothermic DTA peak at 12.

Table 3 depicts the ½ order of reaction with comparative activation energy with its close analog of **CIMP** nickel complex. The enthalpy change is smaller whereas the Gibb's free energy change is large with very negative entropy change. The degradation occurs as shown in Scheme 8:

Compound **6** following the same trend of its analogs, degrades in two steps. The first step starting at 240 °C and completes at 380 °C with the release of two moles of carbon monoxide, one mole each of dihydrogen and dinitrogen gases. This stage is supported by the appearance of one endothermic DTA peak. The second stage starts at 480 °C and completes at 640 °C, releasing the same 4-bromobiphenolate ion with a huge exothermic peak of 40 μV. The residue was calculated to be Co<sub>2</sub>O<sub>3</sub>. The pyrolysis follows infinite order of kinetics and 12.97 kJ/mol of activation energy. The rest parameters are almost following the same trend. The stepwise degradation of **6** is shown in Scheme 9:

Compounds **7** and **8** are following the same trend of degradation with the difference in the starting and ending temperature points. The first step in compound **7** is comprised evolution of two moles carbon monoxide, one mole of dinitrogen and dihydrogen molecules whereas this stage in **8** is marked with the release of two moles of hydrogen cyanide formation along with the release of one mole of chloroform molecule came from solvent of recrystallization. Both the compounds show endothermic DTA peaks for this stage. Stage two in both the compounds is identical with the same parental difference of temperature limits. This stage starts at 280 °C in **7** and at 360 °C in **8** and ends at 640 °C in **7** and 800 °C in **8**. The moiety evolved during this stage is the same 4-bromobiphenolate ion produced by the fusion of the two free radicals. Both these compounds show of –26 and 40 μV in the DTA graph. In **7** the residue remaining was assigned to be copper oxide whereas in **8** the residue was found out to be zinc metal. The former is following 5th order kinetics whereas the latter 3rd order kinetics. The activation energy for **8** is also very high than that of **7**. The rest of the thermodynamic parameters, calculated, are comparable with each other. The degradation of **7** and **8** are shown in Schemes 10 and 11 respectively.

**Scheme 10.** Thermal degradation of **7**.**Scheme 11.** Thermal degradation of **8**.

From the thermal degradation data of the series of meta complexes of **BIMP**, it becomes clear that the order of stability on the basis of Td is Co(II) > Zn(II) > Cu(II) > Ni(II) whereas the order of decreasing activation energy is Ea<sub>8</sub> > Ea<sub>5</sub> > Ea<sub>6</sub> > Ea<sub>7</sub>.

#### 4. Conclusion

Metal complexes of the two very important Schiff base ligands were prepared following different approaches of the synthesis. All the metal complexes were assigned the square planar geometries basing on the results obtained from different analytical and spectroscopic measurements. All the compounds were tested for their inhibiting activities for enzymes like urease, α-chymotrypsin, acetyl cholinesterase, and butyrylcholinesterase. Both the ligands **CIMP** and **BIMP** were found to be active against α-chymotrypsin whereas their copper complexes were found to be active against urease. The rest of metal complexes were found to be inactive against any of the tested enzyme. The unique nature of the copper square planar complexes may be due to the interactions of the complex with carbonyl group of the glycine located on enzyme. This interaction can be established due to the geometric strain in the copper complex, i.e., the complex may either attain square pyramidal or octahedral geometry which is much more favorable than the distorted square planar geometry. All of the compounds are inactive against acetyl cholinesterase and butyrylcholinesterase. Overall based upon the Td values it become clear that the order of stability for the complexes of **CIMP** series is Cu(II) > Co(II) > Ni(II) < Zn(II) whereas based on the activation energies it is clear that Ea<sub>2</sub> > Ea<sub>3</sub> > Ea<sub>1</sub> > Ea<sub>4</sub>. From the thermal degradation data of the series of metal complexes of **BIMP**, it becomes clear that the order of stability on the basis of Td is Co(II) > Zn(II) > Cu(II) > Ni(II) whereas the order of decreasing activation energy is Ea<sub>8</sub> > Ea<sub>5</sub> > Ea<sub>6</sub> > Ea<sub>7</sub>.

#### Acknowledgments

The authors Muhammad Ikram and Sadia Rehman gratefully acknowledge the Higher Education Commission (HEC) Pakistan for financial assistance.

#### Appendix A. Supplementary data

Supplementary data associated with this article can be found, in the online version, at <http://dx.doi.org/10.1016/j.tca.2012.12.023>.

#### References

- [1] H.L.T. Mobley, R.P. Hausinger, Microbial ureases: significance, regulation, and molecular characterization, *Microbiol. Rev.* 53 (1989) 85–108.
- [2] K.W. Leon, J. Jarvik (Eds.), *International Review of Cytology*, Academic Press, San Diego, 1993.
- [3] H.L.T. Mobley, M.D. Island, R.P. Hausinger, Molecular biology of microbial ureases, *Microbiol. Rev.* 59 (1995) 451–480.
- [4] P.E. Wilcox, Chymotrypsinogens—chymotrypsins, *Methods Enzymol.* 19 (1970) 64–108.
- [5] (a) F.A. Cotton, G. Wilkinson, C.A. Murillo, *Advanced Inorganic Chemistry*, Wiley, New York, 1999; (b) M.E. Cuff, K.I. Miller, K.E. van Holde, W.A. Hendrickson, Crystal structure of a functional unit from Octopus hemocyanin, *J. Mol. Biol.* 278 (1998) 855–870; (c) E.I. Solomon, U.M. Sundaram, T.E. Machonkin, Multicopper oxidases and oxygenases, *Chem. Rev.* 96 (1996) 2563–2605; (d) N. Kitajima, Y. Moro-oka, Copper-dioxygen complexes. Inorganic and bioinorganic perspectives, *Chem. Rev.* 94 (1994) 737–757;

- (e) K.A. Magnus, H. Ton-That, J.E. Carpenter, Recent Structural work on the oxygen transport protein hemocyanin, *Chem. Rev.* 94 (1994) 727–735.
- [6] (a) R.H. Holm, P. Kennepohl, E.I. Solomon, Structural and functional aspects of metal sites in biology, *Chem. Rev.* 96 (1996) 2239–2314;  
(b) E.T. Adam, Copper protein structures, *Adv. Protein Chem.* 42 (1991) 145–197;  
(c) S.K. Chapman, in: R.W. Hay, J.R. Dilworth, K.B. Nolan (Eds.), *Perspectives on Bioinorganic Chemistry*, JAI Press, London, 1991, p. 95.
- [7] S. Schindler, Reactivity of copper(I) Complexes towards dioxygen, *Eur. J. Inorg. Chem.* (2000) 2311–2326.
- [8] A. Coblenz, Treatment of geriatric peptic ulcer with chymotrypsin and an antibiotic, *J. Am. Geriatr. Soc.* 16 (9) (1968) 1039–1046.
- [9] M. Arfan, M. Ali, H. Ahmad, I. Anis, A. Khan, M.I. Choudhary, M.R. Shah, Urease inhibitors from *Hypericum oblongifolium* wall, *J. Enzyme Inhib. Med. Chem.* 25 (2010) 296–299.
- [10] R.J.P. Cannell, S.J. Kellam, A.M. Owsianka, J.M. Walker, Results of a large scale screen of microalgae for the production of protease inhibitors, *Planta Med.* 54 (1988) 10–14.
- [11] L. Zhang, S.B. Mulrooney, A.F.K. Leung, Y. Zeng, B.C.K. Ben, R.P. Hausinger, H. Sun, Inhibition of urease by bismuth(III): implications for the mechanism of action of bismuth drugs, *Biomaterials* 19 (2006) 503–511.
- [12] H. Sugimoto, H. Ogura, Y. Arai, Y. Iimura, Y. Yamanishi, Research and development of donepezil hydrochloride, a new type of acetylcholinesterase inhibitor, *Jpn. J. Pharmacol.* 89 (1) (2002) 7–20.
- [13] J.L. Sussman, M. Harel, F. Frolow, C. Oefner, A. Goldman, L. Toker, I. Silman, Atomic structure of acetylcholinesterase from *Torpedo californica*: a prototypic acetylcholine-binding protein, *Science* 253 (5022) (1991) 872–879.
- [14] G.M. Shankar, S. Li, T.H. Mehta, G.A. Arcia-Munoz, N.E. Shepardson, I. Smith, F.M. Brett, F.M.A. Arrell, M.J. Rowan, C.A. Lemere, C.M. Regan, D.M. Walsh, B.L. Sabatini, D.J. Selkoe, Amyloid-beta protein dimers isolated directly from Alzheimer's brains impair synaptic plasticity and memory, *Nat. Med.* 14 (8) (2008) 837–842.
- [15] S. Nochi, N. Asakawa, T. Sato, Kinetic study on the inhibition of acetylcholinesterase by 1-benzyl-4-[(5,6-dimethoxy-1-indanon)-2-yl]methylpiperidine hydrochloride (E2020), *Biol. Pharm. Bull.* 18 (1995) 1145–1147.
- [16] W. Tong, E.R. Collantes, Y. Chen, W.J. Welsh, A comparative molecular field analysis study of N-benzylpiperidines as acetylcholinesterase inhibitors, *J. Med. Chem.* 39 (1996) 380–387.
- [17] Q. Yu, H.W. Holloway, T. Utsuki, A. Brossi, N.H. Greig, Long-acting anti-cholinesterases for myasthenia gravis: synthesis and activities of quaternary phenylcarbamates of neostigmine, pyridostigmine and physostigmine, *J. Med. Chem.* 42 (1999) 1855–1861.
- [18] (a) N.H. Greig, T. Utsuki, Q. Yu, X. Zhu, H.W. Holloway, T. Perry, B. Lee, D.K. Ingram, D.K. Lahiri, A new therapeutic target in Alzheimer's disease treatment: attention to butyrylcholinesterase, *Curr. Med. Res. Opin.* 17 (2001) 159–165;  
(b) M. Ikram, S.-U.-. Rehman, S. Rehman, R.J. Baker, C. Schulzke, Synthesis, characterization and distinct butyrylcholinesterase activities of transition metal [Co(II), Ni(II), Cu(II) and Zn(II)] complexes of 2-[(E)-(quinolin-3-ylimino)methyl]phenol, *Inorg. Chim. Acta* 390 (2012) 210–216.
- [19] (a) P.G. Cozzi, Metal–Salen Schiff base complexes in catalysis: practical aspects, *Chem. Soc. Rev.* 33 (2004) 410–421;  
(b) X.M. Ouyang, B.L. Fei, T.A. Okamuro, W.Y. Sun, W.X. Tang, N. Ueyama, Synthesis, crystal structure and superoxide dismutase (SOD) activity of novel seven-coordinated manganese(II) complex with multidentate di-Schiff base ligands, *Chem. Lett.* (2002) 362;
- (c) C. Jayabalakrishnan, K. Natarajan, Ruthenium(II) carbonyl complexes with tridentate Schiff bases and their antibacterial activity, *Transit. Met. Chem.* 27 (2002) 75–79;  
(d) H. Sharghi, M.A. Nasser, Schiff-base metal(II) complexes as new catalysts in the efficient, mild and regioselective conversion of 1,2-epoxyethanes to 2-hydroxyethyl thiocyanates with ammonium thiocyanate, *Bull. Chem. Soc. Jpn.* 76 (2003) 137–142.
- [20] H. Adams, N.A. Bailey, I.S. Baird, D.E.F. Costes, G. Cros, J.P. Laurent, The syntheses, properties and crystal and molecular structures of the copper(II) and nickel(II) complexes of the non-symmetric schiff bases, derived from 1,2-diaminoethane, pentane-2,4-dione and 2-pyrollecarboxaldehyde, *Inorg. Chim. Acta* 101 (1985) 7–12.
- [21] R. Atkins, G. Brewer, E. Kokot, G.M. Mockler, E. Sinn, Copper(II) and nickel(II) complexes of unsymmetrical tetradentate Schiff base ligands, *Inorg. Chem.* 24 (1985) 127–134.
- [22] B. De Clercq, F. Verpoort, Atom transfer radical polymerization of vinyl monomers mediated by schiff base ruthenium–alkylidene catalysts and the adventitious effect of water in polymerizations with the analogous cationic complexes, *Macromolecules* 35 (2002) 8943–8947.
- [23] T. Opstal, F. Verpoort, Synthesis of highly active ruthenium indenylidene complexes for atom-transfer radical polymerization and ring-opening-metathesis polymerization, *Angew. Chem. Int. Ed.* 42 (2003) 2876–2879.
- [24] T. Opstal, F. Verpoort, ruthenium indenylidene and vinylidene complexes bearing schiff bases: potential catalysts in enol-ester synthesis, *Synlett* 6 (2002) 935–942.
- [25] S.N. Pal, S. Pal, A Diruthenium(III) Complex possessing a diazine and two chloride bridges: synthesis, structure, and properties, *Inorg. Chem.* 40 (2001) 4807–4810.
- [26] B. De Clercq, F. Verpoort, Assessing the scope of the introduction of schiff bases as co-ligands for monometallic and homobimetallic ruthenium ring-opening metathesis polymerisation and ring-closing metathesis initiators, *Adv. Synth. Catal.* 34 (2002) 639–648.
- [27] B. De Clercq, F. Lefebvre, F. Verpoort, Immobilization of multifunctional Schiff base containing ruthenium complexes on MCM-41, *Appl. Catal. A* 247 (2003) 345–364.
- [28] R.I. Kureshy, N.H. Khan, S.H.R. Abdi, S.T. Patel, P. Iyer, Chiral Ru(II) Schiff base complex-catalysed enantioselective epoxidation of styrene derivatives using iododicyclopentadiene as oxidant. II, *J. Mol. Catal. A: Chem.* 150 (1999) 175–183.
- [29] R. Ramesh, Spectral and catalytic studies of ruthenium(III) Schiff base complexes, *Inorg. Chem. Commun.* 7 (2004) 274–276.
- [30] G.L. Ellman, A colorimetric method for determining low concentrations of mercaptans, *Arch. Biochem. Biophys.* 74 (1958) 443–450.
- [31] L. Zhang, S.B. Mulrooney, A.F. Leung, Y. Zeng, B.B. Ko, R.P. Hausinger, H. Sun, Inhibition of urease by bismuth(III): implications for the mechanism of action of bismuth drugs, *Biomaterials* 19 (5) (2006) 503–511.
- [32] X. Dong, Y. Li, Z. Li, Y. Cui, H. Zhu, Synthesis, structures and urease inhibition studies of copper(II) and nickel(II) complexes with bidentate N,O-donor Schiff base ligands, *J. Inorg. Biochem.* 108 (2012) 22–29.
- [33] O. Trott, A.J. Olson, AutoDock Vina: improving the speed and accuracy of docking with a new scoring function, efficient optimization and multithreading, *J. Comput. Chem.* 31 (2010) 455–461.
- [34] H.H. Horowitz, G. Metzger, A new analysis of thermogravimetric traces, *Anal. Chem.* 35 (10) (1963) 1464–1468.
- [35] M. Olszak-Humienik, J. Mozejko, Thermodynamic functions of activated complexes created in thermal decomposition processes of sulphates, *Thermochim. Acta* 344 (2000) 73–79.